Available online at www.sciencedirect.com
ScienceDirect
Trans. Nonferrous Met. Soc. China 25(2015) 2847−2855
Transactions of Nonferrous Metals Society of China
www.tnmsc.cn

Friction stir processing of 7075 Al alloy and subsequent aging treatment

Siavash GHOLAMI, Esmaeil EMADODDIN, Mohammad TAJALLY, Ehsan BORHANI

Faculty of Materials & Metallurgical Engineering, Semnan University, Semnan 35131-19111, Iran

Received 26 October 2014; accepted 14 March 2015

Abstract: The effect of temperatures and time of post-process aging on the microstructure, mechanical properties and wear behavior of friction stir processed 7075 Al alloy was investigated, using optical microscopy (OM), scanning electron microscopy (SEM), transmission electron microscopy (TEM) and Vickers microhardness tester. The results indicate that homogeneous, equiaxed and fine recrystallized microstructure is obtained with the grain size of 4−5 μm. The hardness value increases up to 30% and 80% in the stir zone and the base material, respectively. Based on the TEM observations, it is concluded that the improved properties following the duplex friction stir−aging process can be attributed to the very fine precipitates. Comparing the single and double aging conditions, the hardness of single aging sample is higher than that of double aging one which can be attributed to the high fraction of very fine spheroidal precipitate in single aging sample. The wear rate is reduced by the aging of Al alloy and a more decrease is achieved after the aging of FSPed sample.

Key words: friction stir process; 7075 Al alloy; aging; microhardness

1 Introduction

Al alloys of series 7xxx that are made up of Al−Zn−Mg−Cu are widely used as structural materials due to their relative low density, high strength, ductility, toughness, and fatigue resistance [1−3]. Among these Al series, the 7075 Al alloy is an important material in aircraft structures due to the high specific strength [4]. The strong precipitation strengthening response in 7xxx series alloys in most cases is associated with the nano scale precipitation of metastable η' phase and its precursors [5,6]. By double aging of Al−5Zn−2Mg alloy at high temperatures (at 80 °C for 16 h followed by at 150 °C for 24 h), a slightly coarser precipitate structure is produced. The single stage aging of this alloy at 150 °C for 24 h produces a fine dispersion of intermediate η′ precipitates with wide precipitate-free zones [7].

Severe plastic deformation (SPD) techniques are now widely applied for the production of ultrafine-grained (UFG) microstructures or nanostructure in bulk metals. Extensive studies have been carried out on the effect of SPD processes on the microstructure and especially their effect on the precipitation of age-hardened Al [8−17]. Friction stir welding (FSW) process has been successfully used to weld similar and disimilar materials. Many researches were conducted on the friction stir butt welds of engineering alloys to establish process windows which have been applied in the industrial application successfully [18,19].

It has been reported that in the heat affect zone of FSW, this process has little effect on the size of subgrain and leads to coarsening precipitate and increases precipitate-free zone up to 5 times compared with non FSWed sample [20]. In similar observations, SU et al [21] also found the coarsening of precipitate and the development of precipitate-free zone in 7075-T651 Al alloy. The heat treatment after FSW process leads to a significant restoration of the strength of the joints produced under T651 condition and significantly increases the joint performance [22]. Dynamic recrystallization is another well recognized phenomenon in the friction stir process (FSP) [23]. SU et al [24] produced recrystallized grain in 7075 Al alloy with the size of 100 nm by the fast cooling of friction stir processed sample. Similar results were reported by other researchers. They stated that this microstructure was attributed to the continuous dynamic recrystallization in FSP nugget [25].

Another important aspect of FSP is the fact that the FSP affects the aging behavior of Al alloys which has not been studied. The plastic deformation increases the

Corresponding author: Ehsan BORHANI; Tel: +98-23-33654119; E-mail: ehsan.borhani@profs.semnan.ac.ir
DOI: 10.1016/S1003-6326(15)63910-3

precipitation kinetics in the temperature below 300 °C. This can be attributed to both the increase of number of nucleation sites and the increase of effective diffusion coefficient. At high temperatures, the influence of plasticity on the volume fraction of precipitates is negligible. However, in the presence of deformation during the heat treatment, the precipitate morphology is profoundly modified. In spite that the plastic deformation is carried out before or during the aging treatment, the effect of plastic deformation is observed to be similar [26]. Moreover, the fine grain due to the recrystallization of microstructure can also affect the precipitation kinetics because of high precipitation nucleation sites.

Friction stir processing, the new technique for severe plastic deformation, has been developed according to the basic concepts of friction stir welding. Despite of the high response of 7075 Al alloy to age hardening, because of the novelty of friction stir processing, only a few studies have been carried out on the effects of post aging treatment on the microstructure, size, morphology and distribution of precipitate and properties of age hardenable FSPed alloys. In the present study, duplex FSP−aging process was performed to examine the optimum heat treatment parameters and response to the aging of 7075 Al alloy sheet under various conditions for the possibility of practical use of this alloy.

2 Experimental

2.1 Starting materials

A 7075 Al alloy sheet of 250 mm in length, 50 mm in width and 10 mm in thickness with chemical composition (mass fraction, %) of Al−5.28Zn−2.65Mg−1.10Cu−0.61Si−0.76Fe−0.38Mn was used as the starting material. Some sheets of this alloy were solution treated at (753±3) K for 4 h and then rapidly quenched at room temperature to achieve a super-saturated solid solution. The surfaces of samples were cleaned by acetone. Then the friction stir process was carried out at 1200 r/min and 50 mm/min traverse speed of tool with deviation angle of 3°. H13 tool steel pin in a conical geometry with concave shoulder was selected for this study. The ratio of shoulder diameter to pin diameter was considered to be 4. Figure 1 illustrates the shapes, dimensions and details of tool design.

2.2 Post FSP age hardening

Following FSP, some of the samples were cut in dimensions of 15 mm × 50 mm × 10 mm and then aged in one-step (single aging) and two-step (double aging) states. The details of aging regimes are presented in Table 1.

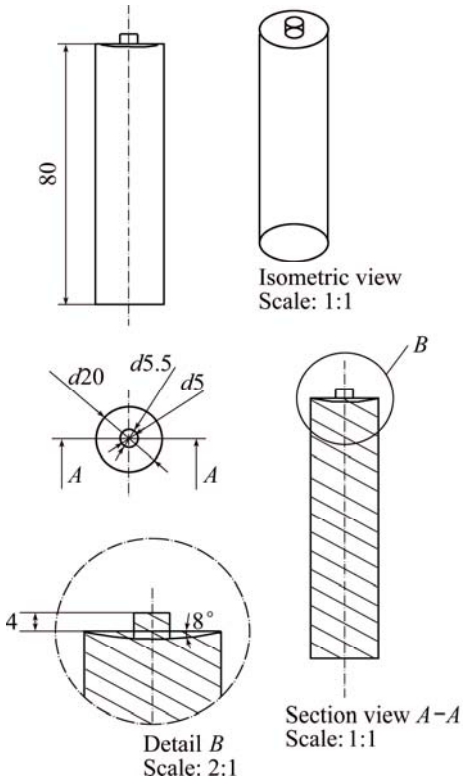

Fig. 1 Dimensions and details of tool design (unit: mm)

Table 1 Aging regime of FSPed samples in one-step and two-step aging

No.	Aging regime
1	One-step aging at 80 °C for 8−96 h
2	One-step aging at 120 °C for 8−72 h
3	One-step aging at 160 °C for 2−16 h
4	Two-step aging: first step at 80 °C for 8 h then increasing the temperature at rate of 2 °C/min and then second step at 140 °C for 4−8 h

2.3 Characterization techniques

The evolution of microstructure was investigated using optical microscopy (OM), scanning electron microscopy (SEM) and transmission electron microscopy (TEM). The metallographic samples were prepared by sectioning the samples using the cut-off wheel machine so as to carry out metallography perpendicular to the FSP direction. The metallographic specimens for the scanning electron microscopy were prepared by mounting and mechanical grinding followed by polishing using alumina powder. Then the samples were etched by using Keller reagent (1% HF + 1.5% HCl + 2.5% HNO_3 + 95% H_2O, volume fraction). The TEM observations were carried out at the voltage of 200 kV. The thin foil specimens were prepared through mechanical polishing down to approximately 70 μm in thickness, and then electro-polishing in the solution of 30% HNO_3 and 70%

CH_3OH before the measurement.

The mechanical properties of specimens were investigated by Vickers microhardness apparatus under a load of 0.15 N on the cross-sections of nugget zone (perpendicular to the FSP direction) at 1 mm distance from the surface. About three measurements were conducted for each hardness data (based on three lines at different cross sections) and the standard deviation was calculated to be approximately ±3.7%.

Dry sliding wear experiments were performed using a pin-on-disk apparatus to evaluate the wear behavior of processed materials against an AISI/SAE 52100 steel disk with a hardness of HRC 60. The heat treated specimens were machined and the pins, 5 mm × 5 mm, were prepared by polishing to 0.5 um. The wear tests were conducted under nominal loads of 30 and 50 N at a constant sliding speed of 1 m/s for a sliding distance of 1000 m and the relative humidity of the atmosphere was hold at (29±2)%. The wear rate was calculated from the mass difference, which was measured before and after each test with a precision of 0.1 mg, divided by the sliding distance. The friction coefficient is determined as the ratio of friction force to normal force. An electrical sensor was used for measuring the friction force.

3 Results and discussion

3.1 Microstructural observation

The microstructures of the base material and the FSPed material of 7075 Al alloy are shown in Figs. 2(a) and (b), respectively.

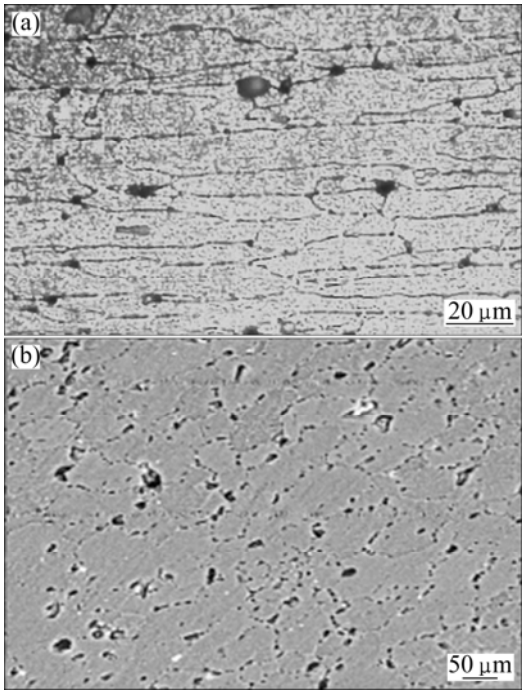

Fig. 2 OM image of raw material (a) and SEM image of FSPed material (b)

The grain size of the samples was determined by the reconstruction of SEM micrograph (Fig. 3(a)), and using MIP software for analyzing the grain structure corresponding to the SEM images (Fig. 3(b)). The grain size of the FSPed sample was measured to be 500 nm while the grain size of primary material is 50−60 μm. Therefore, it is observed that following the FSP, the grain size decreases by 10−12 times compared with the primary microstructure. On the other hand, the microstructure of FSPed specimen consists of equiaxed grains that can be induced during the dynamic recrystallization process. It leads to the refining of microstructure and the induction of fine and equiaxed microstructure with homogeneous distribution of grains. This grain refinement also has been seen in other SPD process reported in the previous study [12,13].

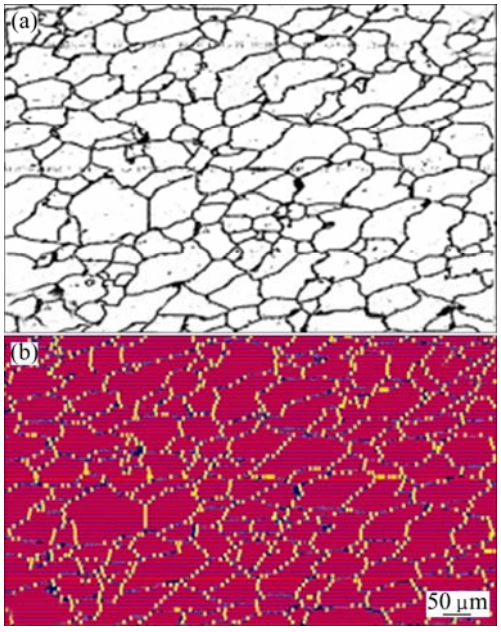

Fig. 3 Reconstructed SEM micrograph of nugget zone after FSP (a) and illustration for analyzing of grain size by MIP software (b)

Figures 4(a) and (b) show the SEM images of the FSPed samples aged at 120 °C and 160 °C for 8 h, respectively. In comparison with the micrograph of FSPed sample (Fig. 2(b)), it can be clearly seen that more and coarser precipitates are formed on the grain boundary by aging treatment, which is responsible for increasing the hardness of alloy. Furthermore, the SEM image in high magnification (Fig. 5(b)) of the FSPed sample aged at 80 °C for 16 h shows many round shaped fine precipitates (white color) which distribute in the matrix and are not seen in the FSPed sample (Fig. 5(a)). It can be attributed to the fine grain due to the friction stir process. Therefore, the friction stir process enhances the grain boundary formation and increases suitable sites for the precipitation of nucleation in aging

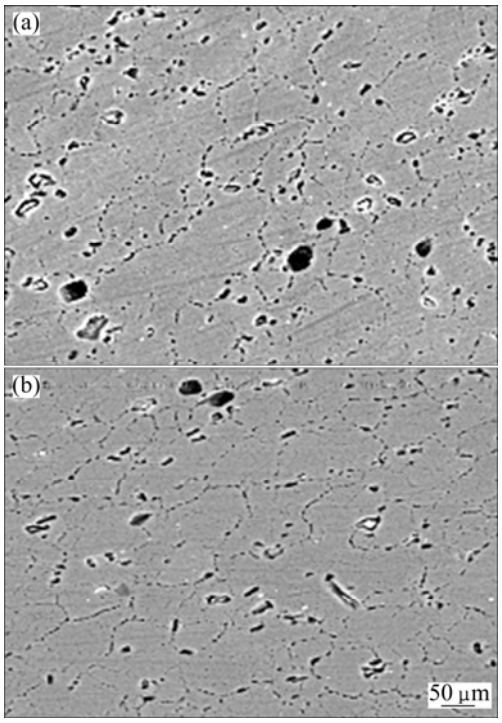

Fig. 4 SEM images of FSPed samples aged at 120 °C (a) and 160 °C (b) for 8 h

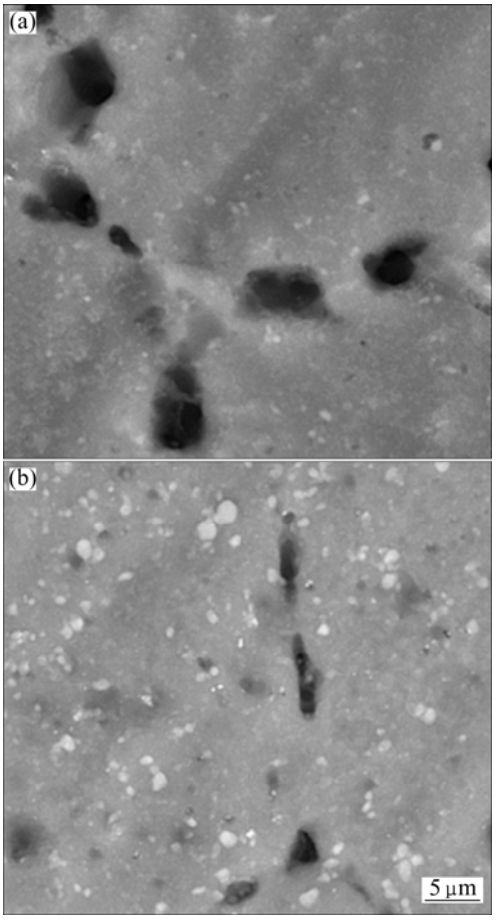

Fig. 5 SEM images of FSPed sample (a) and FSPed sample aged at 80 °C for 16 h (b)

treatment. Some other authors also reported the existence of fine precipitates at the grain boundary of ultrafine grained Al alloy [27−30]. As they reported, the precipitates are distributed along grain boundary in ultrafine grained structure.

3.2 Precipitate size, shape and distribution

3.2.1 Single aging condition

The precipitate characteristics in the one-step aged materials (No. 1 in Table 1) have been shown in the TEM images in Fig. 6. It is observed that the precipitates in the one-step aged specimen have a spherical shape and an average size of 25 nm. Due to aging at low temperature and long holding time, homogeneous nucleation sites are activated in the grain boundary and consequently the precipitate can be formed in the spherical shape within the matrix with a uniform distribution. The presence of spherical precipitate at the grain boundary also has been reported by HU et al [27]. Some coarse precipitates are shown in Fig. 6(b), which have not been dissolved during the solution treatment, therefore the precipitate-free regions are found in adjacent area.

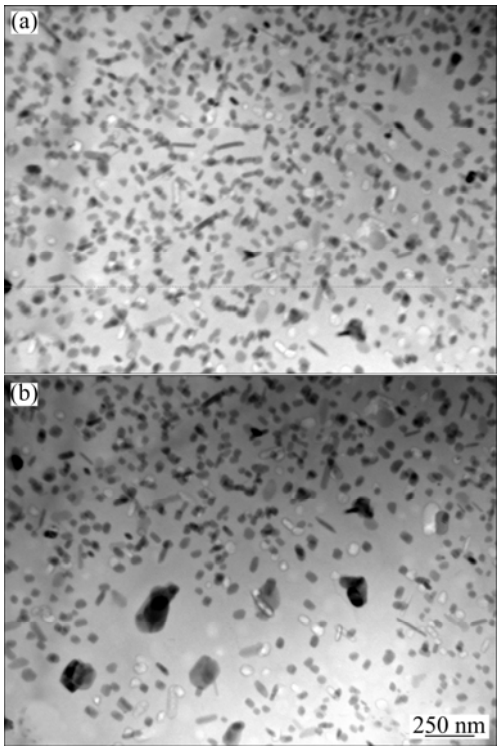

Fig. 6 TEM images of single aging FSPed specimen at 80 °C for 16 h at two different areas

3.2.2 Double aging condition

The precipitates in double aging materials (No. 4 in Table 1) are presented in the TEM images (Fig. 7) presenting both spherical and needle shapes of the nano sized precipitates. The fine needle shape precipitates with an average thickness of 25 nm and an average length of

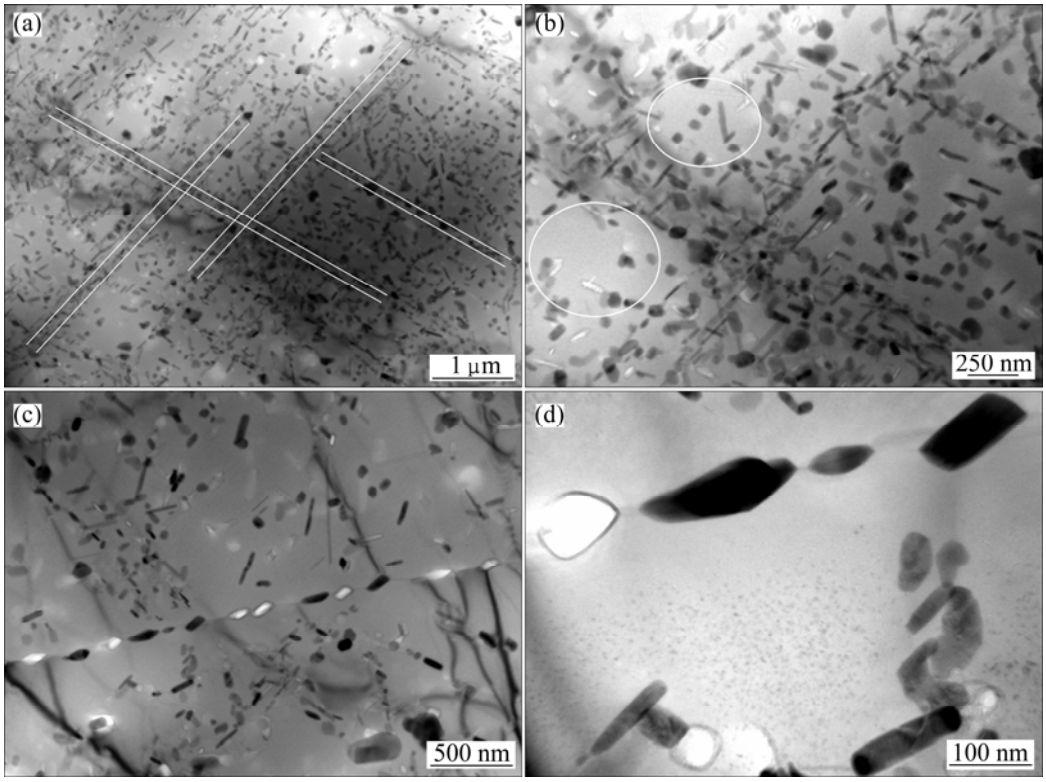

Fig. 7 TEM images of two-step aged materials after FSP: (a) Spherical and needle shape precipitates; (b) Needle shape precipitates along shear bands and spherical shape precipitates along grain boundaries; (c) Low magnification of spherical shape precipitates along grain boundaries; (d) High magnification of spherical shape precipitates along grain boundaries

200 nm are formed in the Al matrix (Fig. 7(a)). These types of precipitates appear in two directions which are perpendicular to each other, indicated by white bands. The formation of parallel band configuration of precipitate in the aged microstructure can be explained. In the first step of aging, the solute atoms move to the shear band which forms during the friction stir processing so that can not act effectively due to low aging temperature and short aging time. This process produces more nucleate precipitate in the shear band. At higher temperature and the second step of aging, the precipitation occurs preferentially along the shear band direction [31,32] and needle shape precipitates are produced (Fig. 7(b)). There are also regions with a few spheroidal precipitates between the shear bands (Fig. 7(b)). During the nucleation of precipitates in the first step, the solute atoms migrate to the shear band as inhomogeneous sites and depleted zones are formed between them. No needle shape precipitates appear in the grain boundary, while spherical shape precipitates are observed in the grain boundary (Figs. 7(c) and (d)).

3.3 Microhardness

3.3.1 Effect of FSP

The microhardness profile of the FSPed sample is shown in Fig. 8. It indicates that FSP increases the hardness especially in the stir zone, therefore the average hardness value of HV 72 in the received material increases to HV 95 in the FSPed material. By moving across the nugget zone, the primary hardness values of the FSPed sample are similar to those of the raw material that proves similar characteristics of FSPed sample with the base metal. This zone is unaffected by the friction stir process. Then the hardness increases with sharp slope to the maximum value. Respecting the tool shoulder diameter equals to 20 mm, it is observed that a zone with

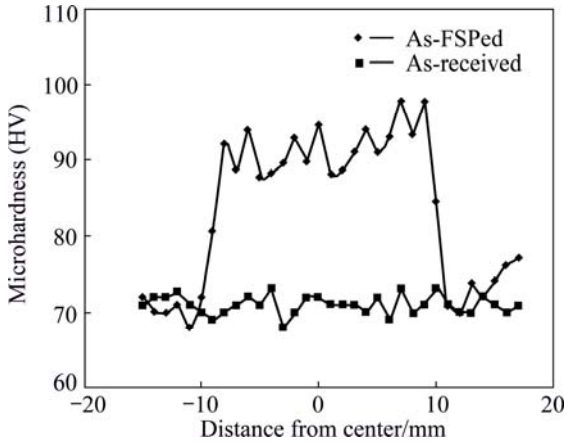

Fig. 8 Microhardness evolution of as-received and FSPed samples in cross-section surface

almost the same length possess the maximum microhardness values.

FSP is one of the SPD processes that produces refined equiaxed grain in microstructure by dynamic recrystallization. Since the mechanical properties such as hardness and strength of materials are relate to the grain size, according to Hull−Petch equation, the hardness in FSP nugget zone increases remarkably compared with that of raw material. SHAERI et al [30] also reported the increase of hardness during the SPD process. It should be noted that the enhancement of hardness in nugget zone by FSP is attributed to the solution treated state instead of the aged state. Otherwise, if processed in the aged-state, the hardness would decrease significantly due to the dissolution of precipitates [22].

3.3.2 Effect of single aging

The microhardness of the FSPed sample is compared with that of the FSP−aged samples at different temperatures for different time under single aging condition for the 7075 Al alloy (Fig. 9). The results indicate that the microhardness is enhanced in both zones

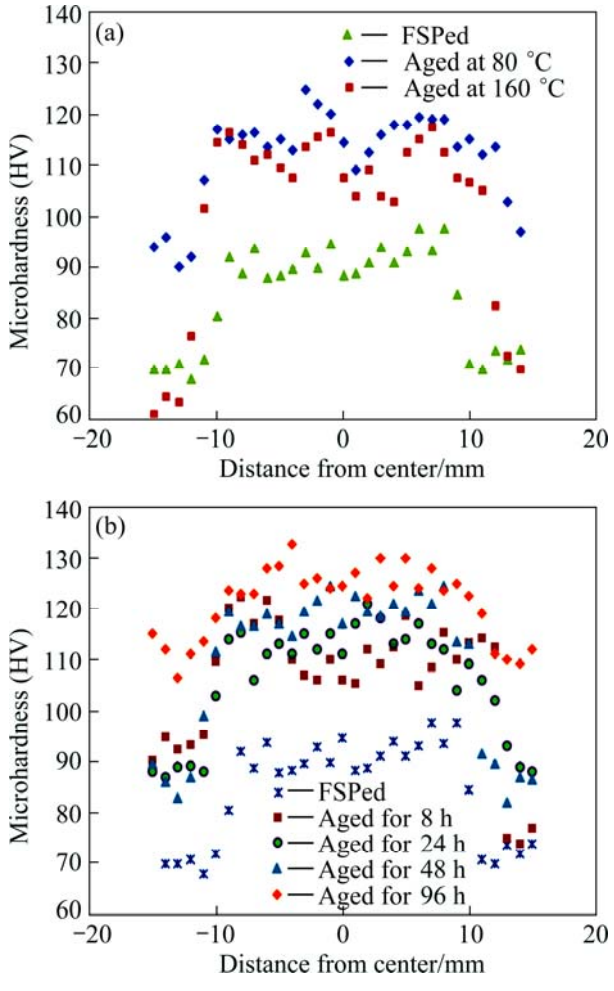

Fig. 9 Distribution of hardness values along FSP zone in samples aged at different temperatures for 16 h (a) and at 80 °C for different time (b)

of substrate and FSP nugget area by increasing the aging time and temperature. It can be attributed to the shape, size and distribution of precipitates. The increase of hardness due to the fine precipitates also has been reported by YAZDIAN et al [33].

The average values of microhardness of nugget zone in different aging conditions are summarized in Fig. 10. It demonstrates that by increasing the temperature, the hardness increases initially and then decreases due to overaging. Similarly, for conger aging time due to the coarsening of precipitates by early overaging, a plateau in the hardness curve is observed, which indicates the lower hardness values.

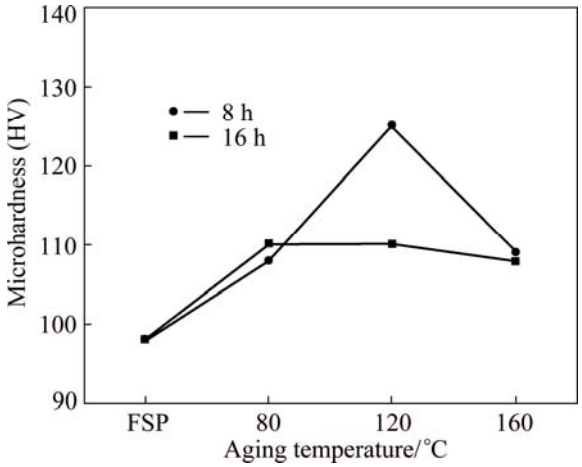

Fig. 10 Variation of average values of hardness in nugget zone versus aging temperatures for 8 h

3.3.3 Effect of double aging

The hardness values of samples with double aging process are given in Fig. 11. It can be observed that the hardness increases initially and then decreases by increasing the holding time in the second step under double aging condition. For the aging time of 4 h, the precipitation is not completed and then the hardness is low, whereas for longer aging time, the metastable η'

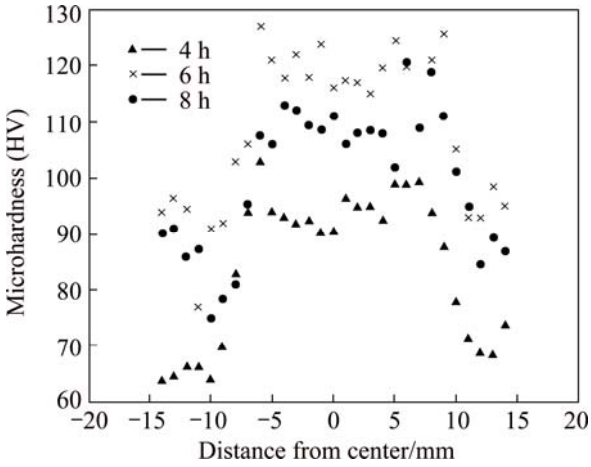

Fig. 11 Distribution of hardness values for samples aged for 4, 6 and 8 h in duplex aging and heating rate after first stage

Table 2 Variation of hardness, wear rate and wear coefficient under different conditions

Sample	*F*=30 N						*F*=50 N					
	Al	SA	DA	FSP	FSP-SA	FSP-DA	Al	SA	DA	FSP	FSP-SA	FSP-D
Hardness (HV)	72	91	89	94	128	110	72	91	89	94	128	110
Wear rate/($mm^3 \cdot N^{-1} \cdot m^{-1}$)	1.67	1.46	1.40	1.32	1.10	1.21	2.96	2.35	2.25	2.10	1.70	1.90
Wear coefficient	4.01	4.43	4.15	4.14	4.69	4.44	4.26	4.28	4.01	3.95	4.35	4.18

phase provides suitable condition of strengthening. Increasing the holding time further, the hardness decreases due to the formation of incoherent precipitate.

The TEM images of single and double aged specimens are shown in Figs. 6 and 7, respectively. The hardness of single aged sample is higher than that of double aged one that can be attributed to high volume fraction of GP-zones and spheroid shape η' precipitates in single aged sample (Fig. 6), whereas the precipitates in double aged sample are coarse plate-like.

3.4 Wear resistance

The variations of wear rate for the samples treated under different conditions are demonstrated in Fig. 12.

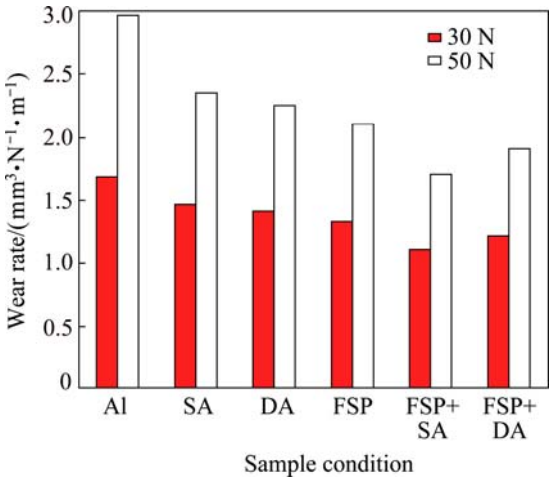

Fig. 12 Variation of wear rate (SA: single aging at 120 °C for 8 h; DA: double aging at 80 °C for 8 h and then at 140 °C for 8 h

The wear rate decreases by artificial aging of Al alloy and it decreases again and again by aging following the FSP process. This behavior can be explained by the grain refinement and the formation of precipitate (Fig. 12). Higher hardness of FSP-aged alloys in comparison with that of raw material (Table 2) may reduce the real contact area, thus reducing the fracture and deformation of the surface asperities.

The wear rate increases by increasing the applied load. Furthermore, the modified alloys by FSP exhibit less wear rate than the un-FSPed alloy. At higher applied load, the increase of temperature due to the frictional heat induces the softening of material, leading to higher wear rate [34].

According to the well-known linear wear law of Archard, the wear rate is inversely proportional to the hardness and directly proportional to the applied load [35]:

$$Q=KW/H \quad (1)$$

where Q is the worn volume per unit sliding distance ($mm^3/(N \cdot m)$), K is the wear coefficient, W is the applied load (N) and H is the Vickers hardness number of the sample. It can be seen that the variation tendency of the wear rate is in accordance with Archard's wear equation and the wear coefficient is calculated to be 4.26.

4 Conclusions

1) The FSP leads to homogeneous microstructure along with equiaxed and fine recrystallized grains which can affect the precipitation phenomenon.

2) The aging induces the hardness to increase by about 30% in stir zone with respect to the as-FSPed material, whereas, the FSP combined with aging treatment results in about 80% improvement in the hardness of base material.

3) The wear rate is reduced by artificial aging of Al alloy, which continues to decrease again and again by aging following the FSP process.

4) Based on the TEM observations, the properties are improved following the duplex FSP−aging process that can be attributed to the precipitation of very fine particles.

5) Comparing the single and double aging conditions, the hardness of single aging sample is higher than that of double aging one that can be attributed to very fine spheroidal precipitate in single aging sample.

Acknowledgements

The authors are grateful to the Department of Material Engineering of Semnan University for improving laboratory facilities.

References

[1] LI Jin-feng, PENG Zhuo-wei, LI Chao-xing, JIA Zhi-qiang, CHEN Wen-jing, ZHENG Zi-qiao. Mechanical properties, corrosion behaviors and microstructures of 7075 aluminum alloy with various aging treatments [J]. Transactions of Nonferrous Metals Society of China, 2008, 18(4): 755−762.

[2] HEINZ A, HASZLER A, KEIDEL C. Recent developments in aluminum alloys for aerospace applications [J]. Materials Science and Engineering A, 2000, 280(1): 102−107.

[3] WILLIAMS J C, STARKE E A. Progress in structural materials for aerospace systems [J]. Acta Materialia, 2003, 51(19): 5775−5799.

[4] LEE W S, SUE W C, LIN C F, WU L J. The strain rate and temperature dependence of the dynamic impact properties of 7075 aluminum alloy [J]. Journal of Materials Processing Technology, 2000, 100: 116−122.

[5] DIXIT M, MISHRA R S, SANKARAN K K. Structure−property correlations in Al 7050 and Al 7055 high-strength aluminum alloys [J]. Materials Science and Engineering A, 2008, 478(1−2): 163−172.

[6] BUHA J, LUMLEY R N, CROSKY A G. Secondary ageing in an aluminium alloy 7050 [J]. Materials Science and Engineering A, 2008, 492(1−2): 1−10.

[7] SMITH W F. Structure and properties of engineering alloys [M]. 2nd ed. New York, USA: Mc-Graw Hill, 1993.

[8] NAKAGAWA K, KANADANI T, TSUJI N, TERADA D, MASUI T, SATO Y. Effect of aging treatment on ultra-fine grains and Si-phase in Al−0.5%Si alloy fabricated by ARB process [J]. Materials Transactions, 2011, 52(10): 1853−1859.

[9] TSAI M S, SUN P L, KAO P W, CHANG C P. Influence of severe plastic deformation on precipitation hardening in an Al−Mg−Si alloy: Microstructure and mechanical properties [J]. Materials Transactions, 2009, 50(4): 771−775.

[10] WAWER K, LEWANDOWSKA M, WIECZOREK A, AIFANTIS E C, ZEHETBAUER M, KURZYDLOWSKI K J. Grain refinement in 7475 aluminum alloy via high pressure to torsion and hydrostatic extrusion [J]. Kovove Materialy-Metallic Materials, 2009, 5: 325−332.

[11] NIKULIN I, KIPELOVA A, MALOPHEYEV S, KAIBYSHEV R. Development of ultra-fine grained structure in an Al−5.4%Mg−0.5%Mn alloy subjected to severe plastic deformation [J]. Materials Transactions, 2011, 52(5): 882−889.

[12] BORHANI E, JAFARIAN H R, TERADA D, ADACHI H, TSUJI N. Microstructural evolution during ARB process of Al−0.2mass% Sc alloy containing Al_3Sc precipitates in starting structures [J]. Materials Transaction, 2012, 53(1): 72−80.

[13] SARKARI KHORRAMI M, KAZEMINEZHAD M, KOKABI A H. Microstructure evolutions after friction stir welding of severely deformed aluminum sheets [J]. Materials and Design, 2012, 40: 364−372.

[14] ÇAM G. Friction stir welded structural materials: Beyond Al-alloys [J]. International Materials Review, 2011, 56(1): 1−48.

[15] ÇAM G, MISTIKOĞLU S. Recent developments in friction stir welding of Al-alloys [J]. Journal of Materials Engineering and Performance, 2014, 23(6): 1936−1953.

[16] İPEKOĞLU G, ÇAM G. Effects of initial temper condition and postweld heat treatment on the properties of dissimilar friction-stir-welded joints between AA7075 and AA6061 aluminum alloys [J]. Metallurgical and Materials Transaction A, 2014, 45(7): 3074−3087.

[17] İPEKOĞLU G, ERIM S, ÇAM G. Effects of temper condition and post weld heat treatment on the microstructure and mechanical properties of friction stir butt welded AA7075 Al-alloy plates [J]. International Journal of Advanced Manufacturing Technology, 2014, 70(1): 201−213.

[18] ZHANG G, SU W, ZHANG J, WEI Z, ZHANG J. Effects of shoulder on interfacial bonding during friction stir lap welding of aluminium thin sheets using tool without pin [J]. Transactions of Nonferrous Metals Society of China, 2010, 20(12): 2223−2228.

[19] LAKSHMINARAYANAN A K, MALARVIZHI S, BALASUBRAMANIAN V. Developing friction stir welding window for AA2219 aluminium alloy [J]. Transactions of Nonferrous Metals Society of China, 2011, 21(11): 2339−2347.

[20] JATA K V, SANKARAN K K, RUSCHAU J J. Friction-stir welding effects on microstructure and fatigue of aluminum alloy 7050-T7451 [J]. Metallurgical and Materials Transactions A, 2000, 31: 2181−2192.

[21] SU J Q, NELSON T W, MISHRA R S, MAHONEY M W. Microstructural investigation of friction stir welded 7050-T651 aluminum [J]. Acta Materialia, 2003, 51: 713−729.

[22] İPEKOĞLU G, ERIM S, GÖREN KIRAL B, ÇAM G. Investigation into the effect of temper condition on friction stir weldability of AA6061 Al-alloy plates [J]. Kovove Materials, 2013, 51(3): 155−163.

[23] HAO D X, LIN W B. Using friction stir processing to produce ultra fine grained microstructure in AZ61 magnesium alloy [J]. Transactions of Nonferrous Metals Society of China, 2008, 18(3): 562−565.

[24] SU J Q, NELSON T W, STERLING C J. A new route to build nanocrystalline materials [J]. Journal of Materials Research, 2003, 18(8): 1757−1760.

[25] RHODES C G, MAHONEY M W, BINGEL W H, CALABRESE M. Fine-grain evolution in friction-stir processed 7050 aluminum [J]. Scripta Materialia, 2003, 48: 1451−1455.

[26] GENEVOIS C, FABREGUE D, DESCHAMPS A, POOLE W J. On the coupling between precipitation and plastic deformation in relation with friction stir welding of AA2024 T3 aluminum alloy [J]. Materials Science and Engineering A, 2006, 441(1−2): 39−48.

[27] HU T, MA K, TOPPING T D, SCHOENUNG J M, LAVERNIA E J. Precipitation phenomena in an ultrafine-grained Al alloy [J]. Acta Materialia, 2013, 61: 2163−2178.

[28] BOBOR K, HEGED Z, GUBICZA J, BARKAI I, PEKKER P, KRALLICS G. Microstructure and mechanical properties of Al 7075 alloy processed by differential speed rolling [J]. Mechanical Engineering, 2012, 56(2): 111−115.

[29] KUMAR S R, GUDIMETLA K, VENKATACHALAM P, RAVISANKAR B, JAYASANKAR K. Microstructural and mechanical properties of Al 7075 alloy processed by equal channel angular pressing [J]. Materials Science and Engineering A, 2012, 533: 50−54.

[30] SHAERI M H, SALEHI M T, SEYYEDEIN S H, ABUTALEBI M R, PARK J K. Microstructure and mechanical properties of Al-7075 alloy processed by equal channel angular pressing combined with aging treatment [J]. Materials and Design, 2014, 57: 250−257.

[31] NG H P, BETTLES C J, MUDDLE B C. Some observations on deformation-related discontinuous precipitation in an Al−14.6at.%Zn alloy [J]. Journal of Alloys and Compounds, 2011, 509(5): 1582−1589.

[32] HUMPHREYS F J, HATHERLY M. Recrystallization and related annealing phenomena [M]. 2nd ed. Oxford, UK: Elsevier, 2004.

[33] YAZDIAN N, KARIMZADEH F, TAVOOSI M. Fabrication and precipitation hardening characterization of nanostructure Al7075 alloy [J]. Indian Journal of Engineering and Materials Science, 2014, 21: 30−34.

[34] ZHANG J, ALPAS A T. Transition between mild and sever wear in aluminum alloys [J]. Acta Materialia, 1997, 45: 513−528.

[35] ARCHARD J F. Contact and rubbing of flat surface [J]. Journal of Applied Physics, 1953, 24: 981−988.

7075 铝合金的搅拌摩擦加工及其后续时效处理

Siavash GHOLAMI, Esmaeil EMADODDIN, Mohammad TAJALLY, Ehsan BORHANI

Faculty of Materials & Metallurgical Engineering, Semnan University, Semnan 35131-19111, Iran

摘　要: 使用光学显微镜、扫描电镜、透射电镜和维氏硬度测定仪研究后处理时效温度和时间对搅拌摩擦加工 7075 铝合金的显微组织、力学性能和耐磨性的影响。结果表明，搅拌摩擦加工可获得均匀的、细小等轴再结晶显微组织，晶粒尺寸为 4~5 μm。在搅拌区域和母材中的硬度值分别增加了 30%和 80%。基于透射电镜观察，推断出摩擦搅拌加工−时效处理对性能的改进归因于细小析出相。比较单一和双重时效条件，发现单一时效样品的硬度高于双重时效样品的硬度，这归因于单一时效样品中高体积分数的细小球状析出相。时效能降低铝合金磨耗率，且搅拌摩擦加工样品时效后其磨耗率降低更多。

关键词: 搅拌摩擦加工；7075 铝合金；时效；显微硬度

(Edited by Mu-lan QIN)